IEEE Access
Multidisciplinary ⋮ Rapid Review ⋮ Open Access Journal

Received 9 October 2023, accepted 12 December 2023, date of publication 9 January 2024,
date of current version 16 January 2024.

Digital Object Identifier 10.1109/ACCESS.2024.3351603

RESEARCH ARTICLE

Route Estimation Toward Autonomous Swimming of Robotic Fish

HIROTAKA TOMI, TAICHI ARAYA, KEISUKE KITANO, (Member, IEEE), KENTA MATSUMOTO, (Member, IEEE), HIROSHI KOBAYASHI, (Member, IEEE), AND TAKUYA HASHIMOTO, (Member, IEEE)
Department of Mechanical Engineering, Tokyo University of Science, Tokyo 162-8601, Japan

Corresponding author: Takuya Hashimoto (tak@rs.tus.ac.jp)

ABSTRACT Underwater robots that imitate aquatic life, such as fish-like robots, have attracted attention for oceanographic studies from the viewpoint of morphological affinity for marine life. The existing studies concerning fish-like robots have primarily focused on the swimming mechanism and locomotive performance, and few studies have been conducted on techniques for self-position estimation and obstacle avoidance despite their indispensability in the autonomous navigation of fish-like robots. Therefore, this study aimed to explore a self-positioning estimation method for robotic fish in an environment where global positioning system (GPS) and pre-defined landmarks are not available. To this end, we first developed a fish-like robot that has a laterally flattened shape, which can mimic the swimming pattern of a fish moving forward by waving a tail fin. Next, we realized the function of simple obstacle avoidance using optical distance sensors for autonomous swimming from a practical perspective. Subsequently, we implemented a real-time swimming-path estimation using the posture derived from the inertial measurement unit (IMU) outputs and the swimming speed measured in advance. Furthermore, a swimming path correction method using a particle filter based on a pre-constructed magnetic map was investigated as an alternative to the GPS correction method. Experiments confirmed the accuracy of the swimming path estimation using the proposed method under various conditions, including obstacle avoidance.

INDEX TERMS Fish-like robot, magnetic map, particle filter, swimming-path estimation, underwater robot.

I. INTRODUCTION

The ocean contains unexplored offshore resources and ecosystems [1]; however, deep-sea activities are hazardous to humans because of the high-water pressure, low oxygen levels, darkness, and cold temperatures. Therefore, underwater vehicles are used for marine operations, such as resource exploration, inspection and maintenance of facilities, and investigation of underwater life. One category of underwater vehicles is unmanned underwater vehicles (UUVs) that are not connected by cables, and some of them are further categorized as autonomous underwater vehicles (AUVs) that perform all operations without human intervention [2], [3]. Although UUVs can potentially contribute to underwater exploration operations, they are insufficient for performing tasks in confined environments. In particular, screw-mounted UUVs have an impact on the surrounding environment such as engulfing seaweed and rolling up sand from the seafloor [4], and marine organisms are cautious around UUVs, making it difficult to study their natural ecosystem.

Underwater robots that imitate aquatic life have been developed to increase the morphological affinity for marine life. Such robots are expected to be employed in oceanographic studies, including data collection for the conservation of underwater environments and endangered species [5]. In particular, the development of fish-like robots that swim by wriggling their bodies and fins instead of using propeller propulsion is noteworthy because of the highly efficient locomotion of fish-like robots in water [6], [7]. As an example of

The associate editor coordinating the review of this manuscript and approving it for publication was Ludovico Minati.

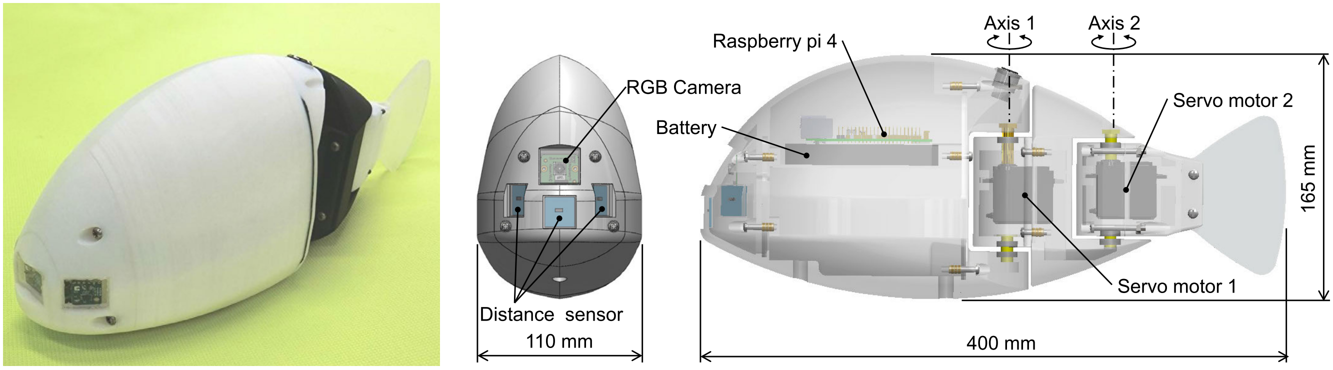

FIGURE 1. Hardware configuration of the fish-like robot.

a fish-like robot, Katzschmann et al. [8] developed a robot, called "SoFi," which has a tail fin made of soft material to realize fish-like tail undulation, to infiltrate into the marine environment for ecological surveys. Two antagonistic hydraulic pumps exist on both sides of the tail, and adjusting the relative pressure of the pumps can generate the turning motion. Its swimming ability has been investigated in the Pacific Ocean, and it has successfully navigated aquatic life at depths ranging from 0–18 m. Yu et al. [9] developed a dolphin-shaped robot that achieved a high propulsion speed of 2.1 m/s with a rotating actuator and rigid link mechanism on two joints in the tail, striving for highly efficient propulsion with a streamlined body that was calculated using a rigid body model. Aubin et al. [10] developed a redox flow battery (RFB) inspired synthetic vascular system and integrated it into a lionfish-like soft robot to increase its energy density. Tomie et al. [11] developed a fish-type micro swimming robot for amusement and educational purposes. The robot was driven by an external magnetic field oscillating with a magnet inside its tail fin. In this way, previous studies on fish-like robots have primarily focused on the development of propulsion mechanisms and the investigation of the effects of tail shape, softness, and movement patterns on swimming speed [12], [13], [14]. However, few studies have been conducted on techniques for self-position estimation and obstacle avoidance, despite their indispensability in autonomous navigation of fish-like robots in terms of practical use.

This study focuses on a self-positioning estimation method in underwater for robotic fish. In general, a global positioning system (GPS) is used to obtain an absolute position on the ground or at sea; however, this technique is limited underwater where electromagnetic waves are attenuated, in addition to indoor. Thus, a method for estimating the self-position using only internal sensors is required for underwater vehicles. For example, an inertial navigation system (INS) is commonly used by an AUV to estimate its position, velocity, direction, and posture. An INS is generally composed of an accelerometer and a gyro sensor to compute the position and posture of the robot without requiring external location information. However, the position data output of the INS contains errors that diverge over time. Therefore, for long-term navigation, the INS output must be corrected using Doppler velocity logging (DVL), which measures speed using sound waves, and acoustic positioning system (APS), which provides positioning through acoustic communication with transponders placed under the sea [15], outside the correction using GPS at sea. However, this kind of equipment is basically too expensive and large to be suitable for robotic fish, and therefore several methods to correct the position and calculate the direction of motion using camera images have been proposed. Zhang et al. [16] employed a Monte Carlo localization (MCL) algorithm that updates the robot position using its distance and direction from a landmark obtained via image processing of camera images and the motion direction and odometry obtained from the inertial measurement unit (IMU). Takada et al. [17] developed a robotic fish equipped with two CMOS cameras and an FPGA. The robot position was estimated using the information obtained from the bottom-facing camera by performing real-time digital image correlation using the FPGA. However, these methods have limitations in that they must be performed in shallow and clear water, and landmarks must be placed beforehand.

As mentioned above, it is still challenging for robotic fish to estimate their own position in environments where transparency is low, or GPS or landmarks are not available. Therefore, in this study, we aimed to explore a method to correct the output of inertial navigation using a pre-constructed geomagnetic map without relying on a camera or marker. To the end, we first developed a fish-like robot that has a laterally flattened shape, which can mimic the swimming pattern of a fish moving forward by waving its tail fin. We then realized a practical function for obstacle avoidance using optical distance sensors for autonomous swimming. Subsequently, we implemented a real-time swimming-path estimation using the posture derived from the IMU outputs and swimming speed that was measured in advance. Next, we examined a method to correct the estimated swimming path using a particle filter with a magnetic map that was constructed in advance. In the experiment, we confirmed the accuracy of the proposed swimming-path

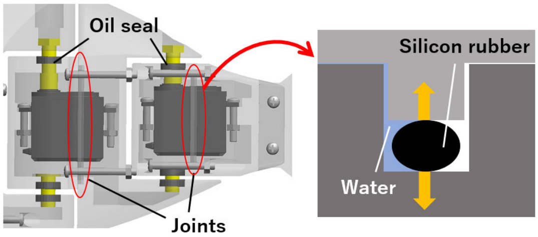

FIGURE 2. Waterproof structure.

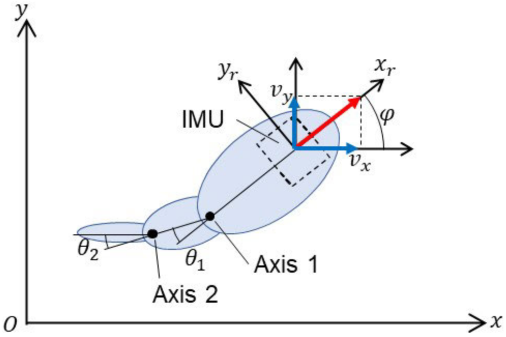

FIGURE 3. Global and local coordinate systems.

estimation method under various conditions, including obstacle avoidance.

II. FISH-LIKE ROBOT

A. HARDWARE CONFIGURATION

The appearance and main components of the developed fish-like robot are shown in Fig. 1. The robot measures 0.400 m × 0.165 m × 0.110 m and weighs 2.1 kg. The hardware can be divided into three units based on the functionality: (a) sensor, (b) power supply and control, and (c) propulsion and turning. The sensor unit on the head is equipped with three laser distance sensors (VL53L0X, ST Microelectronics NV), an RGB camera (IMX219PQ, Sony Co.), and a 9-axis IMU (BNO055, Bosch Co.). The middle upper part's power supply and control unit has an 18.5Wh lithium polymer battery and a Raspberry Pi 4 Model B. The propulsion and turning units have two servomotors for changing the swimming speed and direction. The space below the power supply and control unit is left for the placement of balance weights to control buoyancy, and is also available for implementing the flotation and sinking mechanism in the future.

The housing was 3D-printed with ABS resin, and the tail fin was made of silicone. The openings at the junctions between the housings were designed to be as small as possible to prevent water leakage because large openings are prone to warping due to thermal contraction in FDM-based 3D printing.

As shown in Fig. 2, the junctions were sealed with an O-ring, and an oil seal was inserted into the intersection between the housing and rotation shaft for waterproofing.

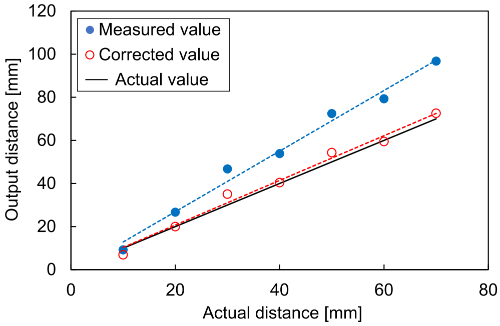

FIGURE 4. Correlation of laser distance sensor.

B. FISH-LIKE SWIMMING

The robot can move straight and turn, mimicking the movement of an actual fish while utilizing the actuation mechanisms of the propulsion and turning unit. This unit enables the robot to propel itself by undulating the trunk and tail joints, in which each joint, Axis 1 and Axis 2, is controlled by different servomotors, as shown in Fig. 3. The rotation angles were adjusted to the desired frequency, amplitude, and phase difference according to Equation (1), as proposed by Hirata [18], to examine the turning performance of the robotic fish.

$$\begin{aligned} \theta_1 &= K_1 A_1^{\max} \sin 2\pi f t, \\ \theta_2 &= K_2 A_2^{\max} \sin(2\pi f t - \phi). \end{aligned} \tag{1}$$

Here, θ_1 [rad] and θ_2 [rad] are the angles of trunk and tail joints, respectively. f [Hz] is the frequency of the cyclic motion, t [s] is the time, and ϕ [rad] is the phase difference between the trunk and tail. $A_1^{\max}$ [rad] and $A_2^{\max}$ [rad] are the maximum amplitudes of the trunk and tail [deg], respectively. K_1 and K_2 are the coefficients representing the degree of amplitude and range from 0–1. Each joint moves symmetrically with respect to the reference plane. When swimming forward, the reference plane is defined at the center of the body and is biased to the left or right when turning. In this way, actuating the two axes independently provides more natural undulation and higher turning capability than a passive movement of spring-coupled tail fin against water resistance [4].

C. OBSTACLE AVOIDANCE USING DISTANCE SENSOR

Avoiding obstacles and tracking objects are also essential functions for autonomous navigation. Therefore, the robot is equipped with a camera and a laser distance sensor to perceive the environment. In this study, we particularly examined simple obstacle avoidance using the distance sensor assuming a situation in which the robot swims along a path where obstacles exist. The sensor measures the distance based on the time-of-flight (ToF) principle, which measures the distance to an object depending on the time difference between the transmission of a signal and its return to the sensor. Since the speed of light attenuates about 75% in water (Fig. 4), we preliminary experimented to determine the relationship

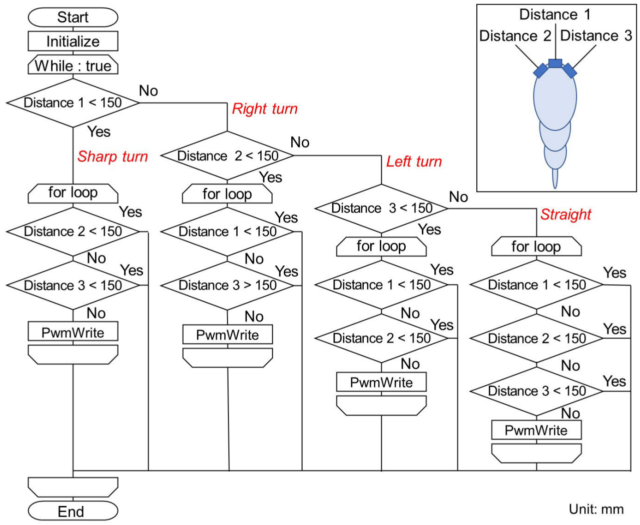

FIGURE 5. Flowchart for obstacle avoidance.

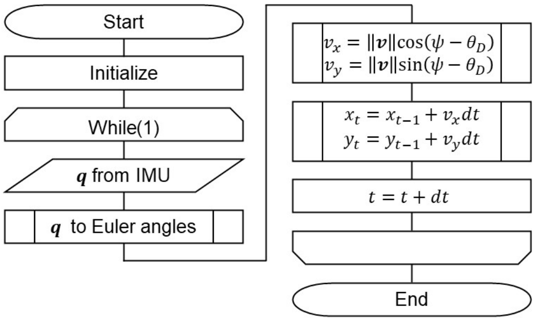
Start
Initialize
While(1)
$\boldsymbol{q}$ from IMU
$\boldsymbol{q}$ to Euler angles
$v_x = \|\boldsymbol{v}\|\cos(\psi - \theta_D)$
$v_y = \|\boldsymbol{v}\|\sin(\psi - \theta_D)$
$x_t = x_{t-1} + v_x dt$
$y_t = y_{t-1} + v_y dt$
$t = t + dt$
End

FIGURE 6. Flowchart for swimming-path estimation using IMU.

between actual distance and the distance output by the sensor. The result shows that the output values of the sensor contain a constant error as shown in Fig. 4. Therefore, we decided to correct the output value of the sensor d using Equation (2) to calculate the actual distance d_c in water.

$$d_c = 0.75d. \tag{2}$$

The obstacle avoidance process assumes the presence of an obstacle and then executes the avoidance algorithm when the distance d_c obtained by at least one of the three sensors is less than 150 mm. The obstacle avoidance process is illustrated in Fig. 5. When an obstacle is detected by the left or right sensor, the centers of vibration of axes 1 and 2 shift by 10° to the left or right, respectively, to avoid the obstacle. When the front sensor detects an obstacle, the center of oscillation of axes 1 and 2 become biased by 10° and 20° to the left and right, respectively, resulting in a sharp turn.

III. SWIMMING-PATH ESTIMATION

A. METHOD OF SWIMMING-PATH ESTIMATION USING IMU

Considering the autonomous navigation of underwater robots, a method with low computational cost and high accuracy is required to localize the self-position of the robot in real-time. Therefore, we investigated inertial navigation using a sensor fusion module based on a 9-axis IMU. The use of this module reduces the computational cost because it contains a microcomputer and directly outputs filter-fused quaternions computed from an accelerometer, gyro sensor, and magnetometer.

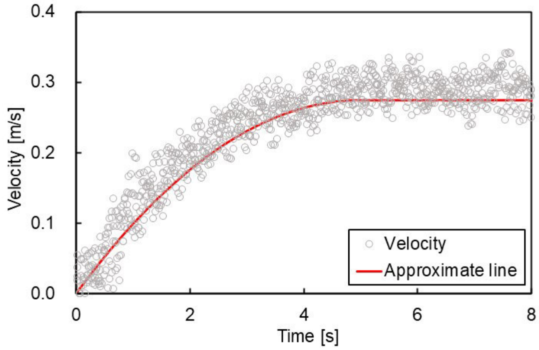

FIGURE 7. Example of velocity change in straight swimming.

TABLE 1. Parameters for approximating velocity change.

Swimming mode	a	b	c	$v_{const.}$
Straight	-0.011	0.110	0.000	0.275
Swing	-0.006	0.060	0.000	0.150

The local and global coordinates are shown in Fig. 3, and Fig. 6 shows the computational flow of the self-position estimation. First, the obtained quaternions $\boldsymbol{q} = (q_w, q_x, q_y, q_z)$ are converted to Euler angles, ϕ, θ, and ψ, using Equation (3).

$$\begin{aligned}
\phi &= \begin{cases} \arctan\left(-\dfrac{2q_yq_z - 2q_xq_w}{2q_w^2 + 2q_z^2 - 1}\right) & (\cos\theta \neq 0) \\ \arctan\left(\dfrac{2q_yq_z + 2q_zq_w}{2q_w^2 + 2q_y^2 - 1}\right) & (otherwise) \end{cases} \\
\theta &= \arcsin\left(2q_xq_z + 2q_yq_w\right) \\
\psi &= \begin{cases} \arctan\left(-\dfrac{2q_xq_y - 2q_zq_w}{2q_w^2 + 2q_z^2 - 1}\right) & (\cos\theta \neq 0) \\ 0 & (otherwise) \end{cases}
\end{aligned} \tag{3}$$

Further, the velocities, v_x and v_y, are calculated in the global coordinates using the yaw angle ψ, the velocity $\boldsymbol{v}$, and the initial head angle θ_D from Equation (4).

$$\begin{aligned} v_x &= \|\boldsymbol{v}\| \cos(\psi - \theta_D) \\ v_y &= \|\boldsymbol{v}\| \sin(\psi - \theta_D) \end{aligned} \tag{4}$$

Here, the norm of velocity $\boldsymbol{v}$ is calculated as follows:

$$\|\boldsymbol{v}\| = v_a + w_v, \tag{5}$$

$$v_a = \begin{cases} at^2 + bt + c & (0 < t \leq 5.0\text{s}) \\ v_{const.} & (t > 5.0\text{s}) \end{cases} \quad [\text{m/s}], \tag{6}$$

where v_a is the average swimming velocity that was experimentally defined in advance and differs for each swimming mode, forward and turning. In the preliminary experiments, the variation in swimming velocity during the acceleration period was obtained, as shown in Fig. 7. Accordingly, the velocity in the acceleration interval was approximated using a polynomial equation of time. Next, the Gaussian noise w_v with a variance of 0.2 was added to represent the velocity fluctuation. Finally, the position in the global coordinate system was calculated using Equation (7).

$$\begin{aligned} x_t &= x_{t-1} + v_x dt, \\ y_t &= y_{t-1} + v_y dt. \end{aligned} \tag{7}$$

Here, (x_t, y_t) and (x_{t-1}, y_{t-1}) are the positions at time t and $t-1$, respectively.

B. CORRECTION USING PARTICLE FILTER BASED ON MAGNETIC MAP

The 3-axis magnetometer installed in an IMU measures the magnetic flux density of geomagnetism as well as that of the residual magnetism derived from the surrounding electronic devices and steel frame of a building. Thus, in an indoor environment, the magnetometer does not indicate the azimuth without calibration. However, the residual magnetism does not fluctuate over time, although it varies depending on the location. Based on this property, researchers have proposed indoor positioning methods for pedestrians and robots using a magnetic map of the surrounding environment recorded in advance [19], [20]. Similarly, if the magnetic map surrounding the robotic fish is obtained in advance, it is used to correct the self-position estimated using the inertial navigation method. Therefore, we investigated a particle filter method combined with a magnetic map to improve the accuracy of the position estimation. In this method, the likelihood of each particle is calculated based on a magnetic map that contains the magnetism of each location, and reliability of the position of the robot is represented by the particle distribution. This process is assumed to be performed between the self-localization using IMU and the time-update described in Fig. 6. The following describes the detailed method for self-localization of the robotic fish using a particle filter in addition to the construction of a magnetic map.

1) SYSTEM MODEL

In the system model, the position of the particle representing the possible position of the robotic fish is calculated from its previous position according to the following equation:

$$\boldsymbol{x}_{t+1}^i = \boldsymbol{x}_t^i + \boldsymbol{v} \cdot dt + \boldsymbol{w}_p, \tag{8}$$

where the position of the i-th particle at time $t+1$ is denoted as $\boldsymbol{x}_{t+1}^i$, and dt is the time step. The vector $\boldsymbol{v}$ is represented as $\boldsymbol{v} = [v_x \; v_y]^T$, where v_x and v_y are calculated using Equation (4), and the values $\boldsymbol{w}_p$ are the Gaussian noise with variance 1. By adding noise to the position and velocity, the beliefs of all the particles were distributed as an ellipsoid with the major axis toward the moving direction of the robot, as shown in Fig. 8. Consequently, the beliefs are adjusted to the robot velocity, even when the robot is accelerating or decelerating at the transition of the swimming mode.

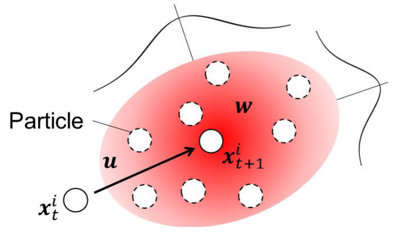

FIGURE 8. Distribution of particle beliefs.

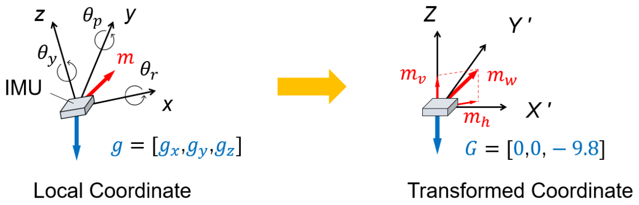

FIGURE 9. Coordinate transformation using posture angle.

2) OBSERVATION MODEL

In the observation model, the likelihood L of each particle is calculated from the magnetic information recorded by the magnetic map and the magnetism measured by the geomagnetic sensor. The probability density function of the Gaussian distribution shown in Equation (9) is used.

$$f(n) = \frac{1}{\sqrt{2\pi\sigma^2}} \exp\left(-\frac{(n-\bar{n})^2}{2\sigma^2}\right), \tag{9}$$

where n corresponds to the magnetism $\boldsymbol{m}^m = \left[m_h^m \; m_v^m \right]^T$ measured by the sensor at time t, $\bar{n}$ is the recorded magnetism $\boldsymbol{m}^r = \left[m_h^r \; m_v^r \right]^T$ of the magnetic map, and σ is the standard deviation of the measured values. Here, the measured magnetism $\boldsymbol{m}^m$ must consistently have the same value at the same location. However, the posture of the IMU mounted on the robot was inconsistent during swimming; hence, the measured magnetic vectors varied depending on the posture, even at the same location. Therefore, the roll angle θ_r and pitch angle θ_p derived from the gravitational acceleration vector were used to transform the posture such that the z-axis of the sensor points in the vertically upward direction as shown in Fig. 9. Because the horizontal and vertical magnetic flux densities do not change with the attitude after the coordinate transformation, they are used as the measured magnetism vector $\boldsymbol{m}^m$. The likelihood was calculated for the horizontal and vertical directions, and their product was defined as the likelihood L of the particle as follows:

$$L = L_h \times L_v. \tag{10}$$

In addition, the likelihoods of all particles were normalized such that the sum becomes 1.

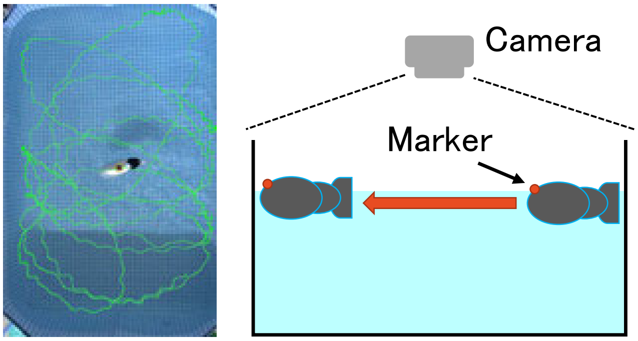

FIGURE 10. Magnetic field-measurement method.

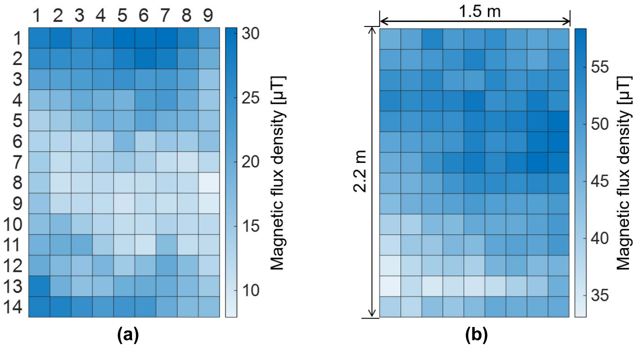

FIGURE 11. Magnetic flux density of experimental environment. Left and right figures show the magnetic flux density in (a) horizontal and (b) vertical directions, respectively.

3) RESAMPLING

To leverage the estimation by a large number of particles in the particle filter, resampling is indispensable to prevent the likelihood of being biased toward a specific particle. Hence, resampling was performed based on the effective sample size (ESS) defined by the following equation:

$$ESS = \frac{1}{\sum_{i=0}^{N} \left(L_t^i\right)^2}. \tag{11}$$

The closer the ESS is to 1, the higher the likelihood of a particular particle and the fewer the number of particles affecting the estimation. Conversely, the closer to the total num ber of particles N, the smaller the difference in likelihood among the particles and the more the particles affect the estimation. The latter is a desirable context for the particle filter; hence, resampling is performed using a low-variance sampling algorithm when the ESS falls below a predefined value.

4) CONSTRUCTION OF MAGNETIC MAP

It is difficult to express the environmental magnetic field surrounding the robotic fish as a function of position, owing to the complicated interference of residual magnetism. Therefore, we experimentally constructed the magnetic map that associates the position to the corresponding magnetism in an experimental field; a small pool measures 2.2 m × 1.5 m as shown in Fig. 10. In the experiment, we first made the robotic fish swim for as long as possible in the pool, and the robot was captured using a camera mounted above the pool, as shown in Fig. 10. The swimming trajectory was then measured by tracking a marker on the robot using image processing software (DIPP-Motion V). A black button switch on the robot head was used as a marker. Subsequently, the trajectory was linked to the magnetism recorded by the magnetometer in the time series, and the horizontal and vertical magnetic flux densities were calculated after coordinate transformation. Finally, the pool was divided into a 14×9 grid, resulting in the side lengths of the grids being approximately 0.16 m, each point on the trajectory was assigned to the one grid that contains it. The mean value and standard deviation of the horizontal and vertical magnetic flux densities of the points contained in the grid were used as the values of magnetism $\boldsymbol{m}^r$ for that grid. Here, the smaller the grid size, the higher the positional accuracy, but the computational cost increases and the number of points in a grid decreases. Considering such a tradeoff and the robot's swimming velocity, the grid size was empirically determined. The magnetic maps constructed in this manner are shown in Fig. 11.

IV. EXPERIMENT ON SWIMMING-PATH ESTIMATION

A. OUTLINE OF EXPERIMENT

Experiments were conducted under three different conditions: straight, circular, and random paths with obstacle avoidance. The experimental environment and measurement method for the swimming trajectory were the same as those in the above experiment for constructing a magnetic map. In addition, the swimming paths were estimated by inertial navigation-based methods using IMU; one used only IMU data, and the other applied a particle filter to correct the inertial navigation. The former was calculated online in real-time during swimming, and the latter was performed offline as a post-processing using the measured data. The initial head angle θ_D of the robot described in Equation (4) was measured via a video analysis.

B. EXPERIMENTAL CONDITIONS

1) STRAIGHT-PATH ESTIMATION

After the robot entered the water at one end of the pool, swimming-path estimation was executed. Both the joint angles, θ_1 and θ_2, were set as 0°, and thus the robot swam forward until it reached the other end for approximately 10 s.

2) CIRCULAR-PATH ESTIMATION

The robot was placed in water at a point 0.1 m along the y-axis and 1.0 m along the x-axis, with the left end of the pool as the origin. The angles of the first and second joints were set as $\theta_1 = 40^\circ$ and $\theta_2 = 20^\circ$, respectively. Additionally, both K_1 and K_2 were set to 0.6. Hence, the robot swam in a clockwise circular orbit.

3) RANDOM PATH ESTIMATION INCLUDING OBSTACLE AVOIDANCE

Six quadrangular rods with 4-cm squared surface were placed inside the pool as obstacles. After entering the water, we made

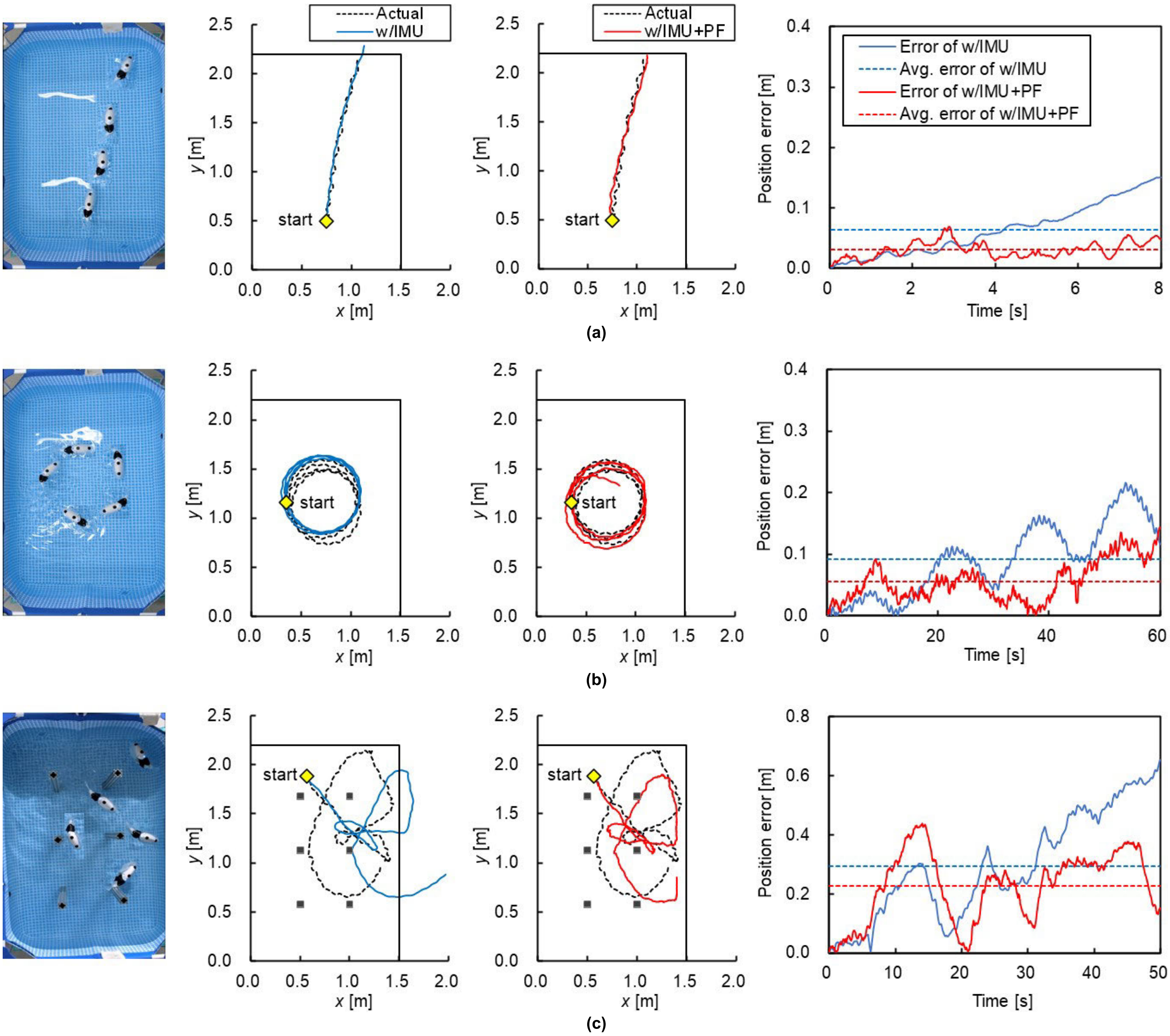

FIGURE 12. Results of swimming-path estimation. (a), (b), and (c) show the results of straight-path estimation, circular-path estimation, and random-path estimation with obstacle avoidance, respectively. In each result, the left picture shows snapshots of the swimming of robotic fish. The two graphs in the middle show a comparison of the actual trajectory and the trajectory estimated by each estimation method. The right graph shows the position erros in each estimation method.

the robot swim toward the nearest obstacle from an arbitrary position and direction. The swimming speed was set as slow as 0.10 m/s such that the robot could avoid obstacles with a sufficient margin. As previously described, when the robot detects an obstacle, it turns to avoid the obstacle smoothly and then swims forward.

V. EXPERIMENTAL RESULT

Fig. 12 shows the results of swimming-path estimation under each condition, where the dot and the red and blue lines represent the true path, the estimated path by the inertial navigation using only IMU data (hereafter referred to as "w/IMU"), and the estimated path corrected by particle filter (referred to as "w/IMU+PF"), respectively. Incidentally, the number of particles in PF was set to 50 in all conditions.

A. STRAIGHT-PATH ESTIMATION

Fig. 12(a) shows the estimation results of straight-path swimming, which indicates that the robot swam approximately 1.8 m in 10 s. Fig. 12(a) shows that the error of w/IMU increases as the swimming distance increases. Conversely, w/IMU+PF suppressed the increase of error as the maximum error was 0.05, resulting in the decrease of the average error from 0.06 to 0.03 m. In straight-path estimation, w/IMU alone provided a high estimation accuracy; however, the accuracy was further improved by correcting the position with the particle filter in w/IMU+PF.

B. CIRCULAR-PATH ESTIMATION

The result of the circular-path estimation is illustrated in Fig. 12(b), which shows that the robot circled four times resulting in the swimming distance of approximately 9 m in 45 s. Similar to the straight-path estimation, w/IMU+PF reduced the average error from 0.1 to 0.05 m. As shown in the figure, the error not only increased in the acceleration interval but also varied periodically with an upward trend according to velocity fluctuations caused by external factors. This is because the robot's trajectory gradually moved despite the constant swimming motion owing to ripple waves and other disturbances accompanied by swimming. The actual trajectory, represented by the red line in Fig. 12(b), gradually shifts downward. As a result, the path estimated by the w/IMU deviated from the actual path because it did not compute the movement caused by disturbances, whereas this influence was suppressed in the w/IMU+PF.

C. RANDOM-PATH ESTIMATION INCLUDING OBSTACLE AVOIDANCE

Fig. 12(c) shows the result of the random-path estimation. The robot swam approximately 6.4 m in 50 s, and its direction changed depending on the measurement patterns of the distance sensors. The actual path (red line) shows that the robot successfully performed obstacle avoidance tasks, even though it sometimes collided with the obstacles and walls. In addition, similar to the previous experiments, the estimation accuracy of w/IMU+PF was improved compared to that of w/IMU; the average error decreased from 0.3 to 0.22 m. Random swimming involves a large variation in acceleration by switching the swimming modes compared to going straight or turning only; hence, the errors increased along with the swimming distance, and their values were higher than those obtained during the previous experiments.

VI. DISCUSSION

In the experiments, the fish-like robot could swim at a maximum speed of 0.25 m/s in the straight-path swimming and perform simple obstacle avoidance in the random swimming. In the evaluation of swimming-path estimation, the comparison of the two methods, w/IMU and w/IMU+PF, revealed that the particle filter effectively reduces the estimation error. One possible cause for the decreasing estimation accuracy is the fluctuation of the acceleration because the estimation method assumes a patterned velocity change. In fact, in the case of w/IMU alone, the estimation error was larger for random swimming, where the velocity was likely to change owing to frequent switching of swimming modes. Meanwhile, w/IMU+PF reduced the error by improving the velocity-change tracking by extending the distribution of particles in the moving direction to improve the tracking of the changes in velocity. Indeed, the experimental results of random swimming showed a smooth transition of the estimated swimming velocity while switching the swimming mode, as shown in Fig. 13. Therefore, it would be effective to adjust the shape of particle distribution depending on swimming mode and posture for further improvement of estimation accuracy. In addition, the number of particles is also considered to affect the accuracy as well as computational load. Fig. 14 shows the error reduction rate and the computation time for each number of particles, which is calculated by MATLAB R2020b on a desktop PC (64-bit Windows 11, 10th generation Intel® Core™ i7-10700, 16GB memory). As the number of particles increases, the error decreases and the computation time increases; however, the error reduction rate becomes saturated above 50, therefore the number of particles in the PF was set to 50 in this study. Furthermore, w/IMU+PF reduces the error caused by drift due to disturbances from the use of a magnetic map; the map represents the absolute position to correct the estimated position of the robot. The proposed method is useful for indoor environments or underwater where GPS data and pre-defined landmarks are unavailable.

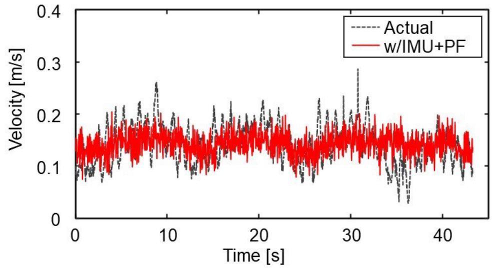

FIGURE 13. Comparison between aculatul velocity and estimated velocitiy with w/IMU+PF in experiment for random-path estimation.

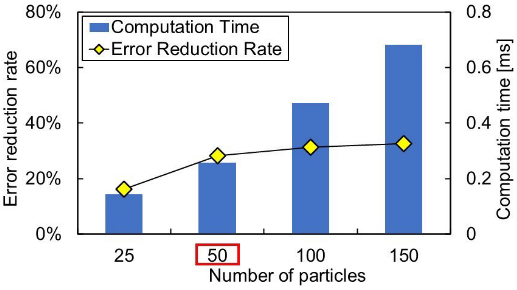

FIGURE 14. Relationship between error reduction rate and computation time varied with the number of particles.

This study demonstrated the feasibility of the autonomous swimming of a fish-like robot that could successfully estimate its own position while avoiding obstacles: the first report of the self-localization method using a magnetic map for small underwater vehicles, particularly robotic fish. However, this study has some limitations and challenges. First, the proposed method requires the construction of a geomagnetic map of the target environment beforehand; hence, it is not applicable to unknown environments. Second, disturbances such as water flow, waves and wind affect the estimation accuracy because our method assumes flat water. To solve this problem, the velocity relative to the water flow must be measured. Third, regarding to swimming performance, although the robot successfully avoided obstacles in most cases at low speeds (approximately 0.1 m/s), it occasionally collided; hence, the probability of collision is considered to be higher if the relative velocity to the obstacle is high or if there are many obstacles around it. Therefore, it is important to detect obstacles from greater distances and to maneuver the robot orientation quickly because collisions also cause a decrease in estimation accuracy. Finally, it is necessary to incorporate the correction process using particle filter into the real-time computation from a practical perspective. To this end, as mentioned above, the number of particles must be optimized in terms of accuracy and computational load with the computational resources available to the robot. Additionally, it is important to address the estimation of three-dimensional swimming paths including floating and sinking.

VII. CONCLUSION

We addressed a swimming-path estimation with obstacle avoidance for a developed fish-like robot. Here, we proposed a correction method for path estimation using magnetic maps and particle filter in environments where GPS and landmarks were not available. Future work will include the improvement of the method for considering the influence of water flow surrounding the robot and the algorithm for obstacle avoidance to further improve the accuracy of path estimation. In addition, we will realize the robot's three-dimensional swimming performance and implement new functions such as environmental sensing, image-based underwater sensing, etc., using RGB camera.

REFERENCES

[1] S. Kang, J. Yu, J. Zhang, and Q. Jin, "Development of multibody marine robots: A review," *IEEE Access*, vol. 8, pp. 21178–21195, 2020.

[2] M. Rogobete and H. International, "An unmanned underwater vehicle defence system," *Sci. Bull. Nav. Acad.*, vol. 1, pp. 16–22, Aug. 2022.

[3] M. Shahrieel, M. Aas, H. A. Kasdirin, M. H. Jamaluddin, and M. F. Basar, "Design and development of an autonomous underwater vehicle (AUV-FKEUTeM)," in *Proc. Malaysian Tech. Universities Conf. Eng. Technol.*, Kuantan, Malaysia, 2009, pp. 1–5.

[4] K. Kugai, I. Yamamoto, Y. Matsumoto, and M. Takahashi, "Development of fish type robot based on the analysis of swimming motion of bluefin tuna-experimental discussion," *J. Aero Aqua Bio-Mech.*, vol. 8, no. 1, pp. 34–40, 2019.

[5] G.-H. Yang, S.-H. Lee, H.-J. Lee, and Y.-S. Ryuh, "Implementation and navigation of a 3-DOF fish robot 'Ichthus V5. 5,'" in *Proc. IEEE Int. Conf. Robot. Biomimetics (ROBIO)*, Guangzhou, China, Dec. 2012, pp. 1045–1049.

[6] R. Salazar, V. Fuentes, and A. Abdelkefi, "Classification of biological and bioinspired aquatic systems: A review," *Ocean Eng.*, vol. 148, pp. 75–114, Jan. 2018.

[7] T. Aritani, N. Kawasaki, and Y. Takada, "Small robotic fish with two magnetic actuators for autonomous tracking of a goldfish," *J. Aero Aqua Bio-Mech.*, vol. 8, no. 1, pp. 69–74, 2019.

[8] R. K. Katzschmann, J. DelPreto, R. MacCurdy, and D. Rus, "Exploration of underwater life with an acoustically controlled soft robotic fish," *Sci. Robot.*, vol. 3, no. 16, Mar. 2018, Art. no. eaar3449.

[9] J. Yu, Z. Su, Z. Wu, and M. Tan, "Development of a fast-swimming dolphin robot capable of leaping," *IEEE/ASME Trans. Mechatronics*, vol. 21, no. 5, pp. 2307–2316, Oct. 2016.

[10] C. A. Aubin, S. Choudhury, R. Jerch, L. A. Archer, J. H. Pikul, and R. F. Shepherd, "Electrolytic vascular systems for energy-dense robots," *Nature*, vol. 571, no. 7763, pp. 51–57, Jul. 2019.

[11] M. Tomie, A. Takiguchi, T. Honda, and J. Yamasaki, "Turning performance of fish-type microrobot driven by external magnetic field," *IEEE Trans. Magn.*, vol. 41, no. 10, pp. 4015–4017, Oct. 2005.

[12] Z. G. Zhang, M. Gondo, N. Yamashita, A. Yamamoto, and T. Higuchi, "Design and control of a fish-like robot using an electrostatic motor," in *Proc. IEEE Int. Conf. Robot. Autom.*, Roma, Roma, Italy, Apr. 2007, pp. 974–979.

[13] H. Y. Luo, "Research and simulation of a flexible robotic fish tail fin propulsion system," in *Proc. Int. Conf. Mechatronics, Manuf. Mater. Eng.*, vol. 63, 2016, p. 01043.

[14] S. Kobayashi, M. Nakabayashi, and H. Morikawa, "Bioinspired propulsion mechanism in fluid using fin with dynamic variable-effective-length spring," *J. Biomechanical Sci. Eng.*, vol. 1, no. 1, pp. 280–289, 2006.

[15] T. Hyakudome, T. Aoki, T. Murashima, S. Tsukioka, H. Yoshida, H. Nakajoh, T. Ida, S. Ishibashi, and R. Sasamoto, "Key technologies for AUV," in *Proc. OCEANS*, vol. 1, Biloxi, MI, USA, 2002, pp. 162–166.

[16] J. Zhang, W. Wang, G. Xie, and H. Shi, "Camera-IMU-based underwater localization," in *Proc. 33rd Chin. Control Conf.*, Nanjing, China, Jul. 2014, pp. 8589–8594.

[17] Y. Takada, K. Koyama, and T. Usami, "Position estimation of small robotic fish based on camera information and gyro sensors," *Robotics*, vol. 3, no. 2, pp. 149–162, Apr. 2014.

[18] K. Hirata, "Development of experimental fish robot," in *Proc. 6th Int. Symp. Mar. Eng.*, Tokyo, Japan, 2000, pp. 711–714.

[19] Y. Li, Y. Zhuang, H. Lan, P. Zhang, X. Niu, and N. El-Sheimy, "WiFi-aided magnetic matching for indoor navigation with consumer portable devices," *Micromachines*, vol. 6, no. 6, pp. 747–764, Jun. 2015.

[20] H. Wu, S. He, and G. S. H. Chan, "Efficient sequence matching and path construction for geomagnetic indoor localization," in *Proc. Int. Conf. Embedded Wireless Syst. Netw.*, Uppsala, Sweden, 2017, pp. 156–167.

HIROTAKA TOMI received the B.S. degree in mechanical engineering from the Tokyo University of Science, Tokyo, Japan, in 2022, where he is currently pursuing the M.S. degree in mechanical engineering.

TAICHI ARAYA received the B.S. and M.S. degrees in mechanical engineering from the Tokyo University of Science, Tokyo, Japan, in 2021 and 2023, respectively.

KEISUKE KITANO (Member, IEEE) received the B.S., M.S., and Ph.D. degrees in mechanical engineering from Doshisha University, Kyoto, Japan, in 2014, 2016, and 2019, respectively. He was a JSPS Research Fellow and an Assistant Professor with Doshisha University, from 2018 to 2020 and from 2020 to 2023, respectively. He is currently an Assistant Professor with the Department of Mechanical Engineering, Tokyo University of Science, Tokyo, Japan. His research interests include sensor fusion, finger dexterity, and biomechanics.

KENTA MATSUMOTO (Member, IEEE) received the B.S., M.S., and Ph.D. degrees in mechanical engineering from Doshisha University, Kyoto, Japan, in 2013, 2015, and 2018, respectively. From 2018 to 2019, he was a Research Fellow with Doshisha University. He is currently an Assistant Professor with the Department of Mechanical Engineering, Tokyo University of Science, Tokyo, Japan. His research interests include biomechanics, sports engineering, wearable device, and welfare robot.

HIROSHI KOBAYASHI (Member, IEEE) received the B.S., M.S., and Ph.D. degrees in mechanical engineering from the Tokyo University of Science, Tokyo, Japan, in 1990, 1992, and 1995, respectively.

From 1992 to 1995, he was a JSPS Postdoctoral Fellow with the Tokyo University of Science. From 1996 to 1998, he was a JSPS Postdoctoral Fellow for foreign study with Zurich University, Zürich, Switzerland. He was appointed as a Lecturer, in 1998, an Assistant Professor, in 1999, and a Professor, in 2008 (to date) with the Department of Mechanical Engineering, Tokyo University of Science. He founded Innophys Company Ltd., in 2013, which is the manufacture and distributer of Muscle Suit®. His current research interests include practical robot system, human interface, affective communication, welfare robot, intelligent image processing, and android robot.

TAKUYA HASHIMOTO (Member, IEEE) received the B.S., M.S., and Ph.D. degrees in mechanical engineering from the Tokyo University of Science, Tokyo, Japan, in 2004, 2006, and 2009, respectively. He is currently an Associate Professor with the Department of Mechanical Engineering, Tokyo University of Science. His research interests include robotics, human–robot interaction (HRI), HRI evaluation, sociability of robots, welfare robots, and human interface.